Available online at www.sciencedirect.com
ScienceDirect
Scripta Materialia 56 (2007) 693–696
Scripta MATERIALIA
www.actamat-journals.com

Damage tolerance of an elastic-brittle diamond-celled honeycomb

I. Quintana Alonso and N.A. Fleck*

Department of Engineering, Cambridge University, Trumpington Street, Cambridge CB2 1PZ, UK

Received 7 November 2006; accepted 20 December 2006
Available online 23 January 2007

The fracture strength of an elastic-brittle, centrally cracked plate made from a diamond-celled lattice is calculated by finite element simulations. Conventional linear elastic fracture mechanics applies when the crack length much exceeds the cell size. But when the crack is only a few cell sizes, the stress concentration at the crack tip is negligible and the strength is comparable to the unnotched strength. An analytical model is derived for the fracture toughness.

Keywords: Finite element analysis; Fracture; Toughness; Elastic behaviour; Honeycomb

Ceramic honeycombs with the square cells shown in Figure 1 are commonly used in catalytic converters and in particulate filters for automobiles. Ceramic foams and honeycombs also find application as filters for liquid metal due to their high chemical stability up to a high temperature. More recently, ceramic lattice materials and other types of brittle honeycombs have also been developed for bioengineering purposes, such as prosthetic scaffold implants. Tailoring the porosity of these structures allows for ingrowth of new bone tissue and also reduces problems associated with the mismatch of elastic properties. The brittle nature of ceramic honeycombs, together with the severe thermal shock and mechanical loads to which they are subjected, makes their damage tolerance a concern.

Early work on the fracture behaviour of brittle honeycombs made use of linear elastic fracture mechanics (LEFM) concepts to estimate the fracture toughness of a hexagonal honeycomb [1]. The stress field of an equivalent linear elastic continuum was used to calculate the stresses on the cell walls of the lattice directly ahead of the crack tip. The macroscopic fracture toughness was estimated by assuming that the critical strut directly ahead of the crack tip fails when the maximum tensile stress within it attains the fracture strength σ_f. These ideas were extended and refined by Huang and Gibson [2] for hexagonal and diamond-celled honeycombs to account for the statistical nature of the modulus of rupture σ_f of the cell-wall material. Huang and Gibson concluded that the fracture toughness of the diamond-celled honeycomb scales as $K_{IC} \propto (t/\ell)^2$, where t is the thickness of each strut and ℓ is its length. We shall reassess this result below for the diamond-celled honeycomb.

Recently, Fleck and Qiu [3] have made numerical and analytical predictions for the fracture toughness of several isotropic honeycombs: hexagonal, triangular and Kagome. They considered both semi-infinite cracks and finite cracks within a centre cracked panel. In the absence of a crack, the panel (with diamond-celled honeycomb microstructure) has an unnotched tensile strength σ_u which scales with the tensile strength of the solid σ_f and with the ratio $\bar{t} = t/\ell$, according to [4]:

$$\sigma_u = \frac{2}{3}\bar{t}^2\sigma_f. \tag{1}$$

Now introduce a macroscopic crack into the honeycomb. At long crack lengths, the strength is dictated by the criterion of linear elastic fracture mechanics, $K_I = K_{IC}$, where K_I is the applied mode I stress intensity factor and K_{IC} is the mode I fracture toughness of the lattice material. Fleck and Qiu [3] showed that the transition in behaviour from *strength-control* to *toughness-control* occurs at the transition flaw size of $a_T = K_{IC}^2/\pi\sigma_u^2$, in agreement with previous studies on fully dense specimens (see e.g. the review by Fleck et al. [5]).

In the present study, we explore the tensile fracture response of a centre-cracked plate (CCP) made from a diamond-celled honeycomb (Fig. 1). The plate contains a crack of length $2a$ and the honeycomb is made from a solid of Young's modulus E_s and tensile fracture strength σ_f. The diamond-celled lattice (sketched in Fig. 2) is characterised by its cell size ℓ, wall thickness

* Corresponding author. Tel.: +44 1223 748240; fax: +44 1223 765046; e-mail: nafl@cam.ac.uk

1359-6462/$ - see front matter
doi:10.1016/j.scriptamat.2006.12.027

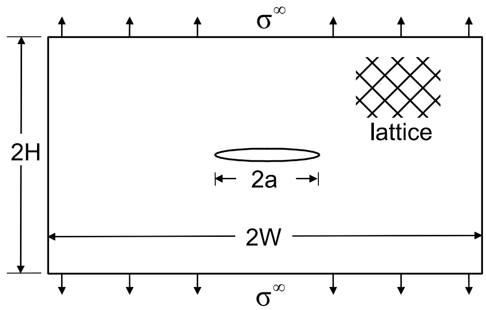

Figure 1. Centre cracked plate (CCP) made from a diamond-celled lattice and subjected to uniaxial tension.

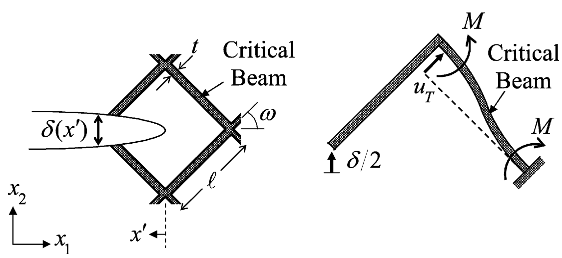

Figure 2. Sketch of the crack tip showing the idealised model of the deformation.

t and core angle ω (only square cells of $\omega = 45°$ are considered in this study). The cell wall material is assumed to be linear elastic up to fracture. The relative density of the diamond-celled lattice as defined by the density of the lattice divided by that of the solid from which the cell walls are made is given by

$$\bar{\rho} = \frac{t}{\ell}\left(2 - \frac{t}{\ell}\right). \tag{2}$$

Throughout this study, the cell size ℓ is held constant and we evaluate the sensitivity of the macroscopic strength to relative density, as parameterised by $\bar{t} = t/\ell$, and to the relative crack length a/ℓ. The specimen width W and height H are taken to be sufficiently large in relation to the crack length for specimen size effects to be negligible. Consequently, the K-calibration for the homogeneous, orthotropic CCP can be taken as $K = \sigma^{\infty}\sqrt{\pi a}$.

The outline of the paper is as follows. An analytic estimate for the fracture toughness of the lattice K_{IC} is derived. The dependence of notched strength of the CCP is explored for a wide range of t/ℓ and a/ℓ by the finite element (FE) method. The notched strength is compared with the unnotched strength at short crack lengths, and with the LEFM prediction at long crack lengths. The role of the T-stress in influencing the fracture strength is also addressed.

Consider the cracked lattice shown in Figure 2. Assume that the bar immediately ahead of the crack tip is the critical bar of the lattice: it fails first. Further, assume that it deforms as a built-in beam, as sketched in Figure 2. The clamping moment M on this bar is

$$M = \frac{1}{2}E_s\frac{t^3}{\ell^2}u_T, \tag{3}$$

where the transverse displacement, u_T, is related to the crack tip opening displacement, δ, evaluated at a distance $x' = \ell/\sqrt{2}$ from the crack tip according to

$$u_T = \frac{\delta(x' = \ell/\sqrt{2})}{2\sqrt{2}}. \tag{4}$$

Recall that the crack tip opening displacement of an equivalent orthotropic continuum is given [6] by

$$\delta(x') = \frac{8}{\sqrt{2\pi}}CK_I\sqrt{x'}, \tag{5}$$

where the elastic coefficient, C, for an orthotropic solid is given in Ref. [7]. For the orthotropic lattice under consideration, C is given by

$$C \simeq \frac{1}{\sqrt{2}E_s\bar{t}^2}. \tag{6}$$

Now assume that this critical beam fails when the local bending stress of $\sigma_A = 6M/t^2$ attains the fracture strength of the cell wall material σ_f. Consequently, from Eqs. (3)–(7), we obtain

$$K_{IC} = \beta\sigma_f\bar{t}\sqrt{\ell}, \tag{7}$$

where the numerical constant $\beta = 1/2$. Numerical investigations [N.E. Romijn and N.A. Fleck, private communication] confirm the scaling of Eq. (11) with only a minor correction to the constant β of $\beta = 0.44$. Note that the linear dependence of K_{IC} upon $\bar{t}$ contrasts with the quadratic dependence for hexagonal honeycombs [1,3], and with the dependence argued previously by Huang and Gibson [2] for a diamond-celled honeycomb.

A simple analytical estimate can be made for the transition flaw size a_T, at which the notched strength of the CCP switches from the unnotched value σ_u to the LEFM value

$$\sigma_c = K_{IC}/\sqrt{\pi a}. \tag{8}$$

The transition length follows from Eq. (7) as

$$\frac{a}{\ell} = \frac{9}{16\pi}\frac{1}{\bar{t}^2}. \tag{9}$$

Note that the transition length scales as ℓ, but is very sensitive to $\bar{t}$. At small $\bar{t}$, such as 1%, we have a long transition crack length, $a_T = 1790\ell$.

Finite element simulations have been performed to determine the fracture strength σ_c of elastic-brittle CCP made from a diamond-celled honeycomb. The commercial finite element code ABAQUS (version 6.5-3) was used. Each strut in the lattice was modelled by a two-noded Euler–Bernoulli beam element (element type $B23$ in ABAQUS notation), which uses cubic interpolation functions and accounts for both stretching and bending deformation but neglects shear deformation. Two ways of introducing a crack into the lattice have been considered (Fig. 3). Crack morphology I has broken bars on each face of the crack (see Fig. 3a). Crack morphology II has intact bars but the joints are split on the crack plane (see Fig. 3b).

The net-section strength σ_c of the CCP is plotted against $(\bar{t}^2a/\ell)$ in Figure 4. This net strength has been normalised by the unnotched strength of the lattice

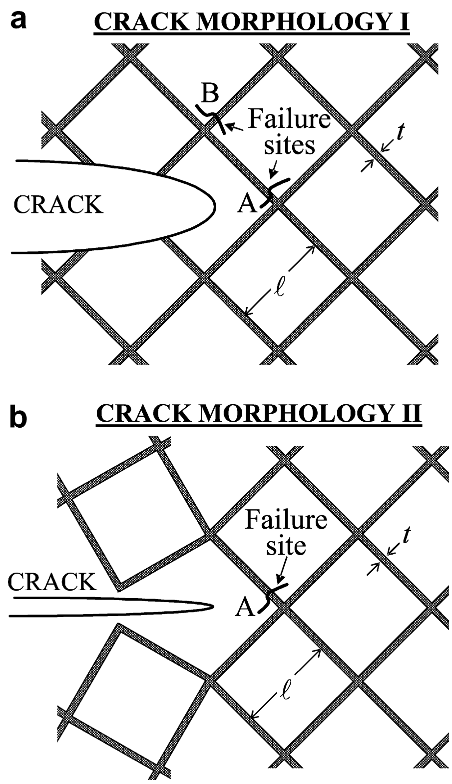

Figure 3. Sketches of the two types of crack morphology.

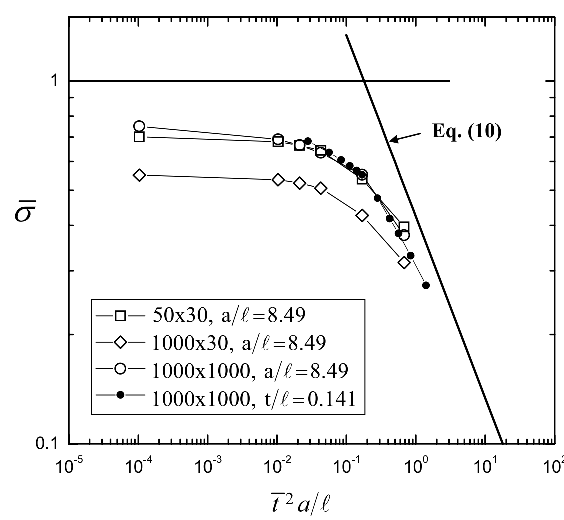

Figure 4. Net strength of the centre cracked plate under uniaxial tension. All simulations are for crack morphology I. The left-most datum point refers to the limit $a/\ell = \sqrt{2}$ for the case $t/\ell = 0.141$.

and is designated $\bar{\sigma}$. The choice of ordinate $(\bar{t}^2 a/\ell)$ is used because the notched strength in the LEFM regime scales according to

$$\bar{\sigma} = \frac{\sigma_c}{\sigma_u} = \frac{3}{4\sqrt{\pi}}(\bar{t}^2 a/\ell)^{-1/2} \tag{10}$$

upon neglecting the minor correction factor $(1 - a/W)$ for the net section, and upon invoking Eqs. (1), (7) and (8).

Numerical results for three grid sizes are shown in Figure 4. The analysis carried out by Huang and Gibson [2] using a grid of 50×30 cells is reproduced. The calculation is repeated for a larger mesh of width 1000 cells and height again of 30 cells. Additionally, a large square grid of dimension 1000×1000 cells is analysed. Simulations have been performed over a wide range of relative density, as parameterised by $\bar{t}$ in the range 0.0035–0.283.

Two regimes of behaviour are evident for each grid (Fig. 4). Above the transition value $(\bar{t}^2 a/\ell) = 9/16\pi$ the strength of the lattice is toughness-controlled: LEFM applies and $\bar{\sigma}$ scales with the combined parameter $(\bar{t}^2 a/\ell)$. Below the transition value, the strength of the lattice is strength-controlled: σ_c is close to the unnotched value σ_u, and so $\bar{\sigma} \approx 1$. Note that the data for varying a/ℓ and $\bar{t}$ held fixed are in good agreement with the data for varying $\bar{t}$ and a/ℓ held fixed when the axes of Figure 4 are used. Huang and Gibson [2] assumed values for $(\bar{t}^2 a/\ell)$ such that their results (labelled 50×30 in Fig. 4) lie in the strength-controlled regime, and so the strength scales as $\bar{t}^2$. It is clear from the present study that their results pertain to the regime of strength-control.

We note from Figure 4 that the 1000×30 mesh is substantially weaker than the 1000×1000 mesh. Consequently, the good agreement between the results for the 50×30 mesh and the 1000×1000 mesh is fortuitous. We conclude that a mesh of 1000×1000 cells is required to give reliable results. Additional numerical experimentation was used to confirm this using a somewhat larger mesh than 1000×1000 cells.

The active failure site (labelled A and B in Fig. 3) within the lattice depends upon the magnitude of $(\bar{t}^2 a/\ell)$ as follows. For crack morphology I the critical site is A within the regime of K-field dominance $(\bar{t}^2 a/\ell > 9/16\pi)$ but switches to B in the strength-controlled regime $(\bar{t}^2 a/\ell < 9/16\pi)$. On the other hand, failure is always at site A for crack morphology II. The sensitivity of failure strength to choice of crack morphology is shown in

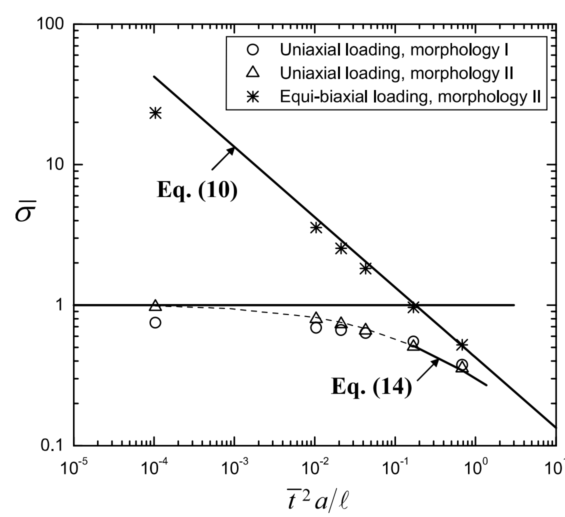

Figure 5. Net strength of the centre cracked plate subjected to uniaxial tension and to equi-biaxial tension. The crack length is held constant at $a/\ell = 8.49$ and the parameter $\bar{t}$ is varied. The grid size is 1000×1000 cells.

Figure 5. For uniaxial tension, crack morphology II is slightly stronger than morphology I in the strength-controlled regime, $\bar{t}^2 a\ell < 9/16\pi$.

The T-stress is defined as the second term in the series expansion of stress in the crack tip field. It is a spatially uniform stress component σ_{11} in the axes of Figure 2. The T-stress scales with the remote applied stress and its magnitude depends upon the specimen geometry of interest (see e.g. [8]). Sih et al. [6] find that the T-stress for a finite crack in an infinite, orthotropic solid scales with the remote applied stress σ^∞ as $T \approx -\sigma^\infty$, independent of the degree of orthotropy.

The significance of the T-stress lies in the fact that it can influence the fracture strength of the solid containing a short crack: at short crack lengths, the T-stress contribution to the near tip stress field is significant. Since the level of T-stress is dependent upon the choice of specimen geometry, the value of fracture toughness deduced from the measured fracture strength displays a dependence upon specimen configuration at short crack lengths. Fleck and Qiu [3] have demonstrated the importance of including T-stress effects in the prediction of fracture strength of three isotropic lattice materials. We explore here the role of the T-stress for the diamond-celled honeycomb.

Recall that, for the CCP under uniaxial loading, the T-stress is given by $T \approx -\sigma^\infty$. Superposition of a remote direct stress $\sigma_{11} = \sigma^\infty$ constitutes equi-biaxial applied loading, and the net T-stress then vanishes. Consequently, the role of the T-stress upon the fracture strength of the CCP can be deduced by comparing the strengths for uniaxial and biaxial loadings. This comparison is made in Figure 5 for the crack morphology II, as defined in Figure 3b. A major T-stress effect is evident at short crack lengths.

The model developed above for the fracture toughness can be modified to include the effect of a non-vanishing T-stress. Consider failure at site A of crack morphology II (Fig. 3b). The local bending stress σ_A at this site is due to the superposition of the singular K-field and the T-stress. The contribution to σ_A from the T-stress is

$$\sigma_A = 1.5\frac{T}{\bar{t}^2}. \tag{11}$$

We note in passing that Eq. (11) is identical to Eq. (1). The net value for σ_A follows from Eqs. (7) and (11) as

$$\sigma_A = \frac{2K_I}{\bar{t}\sqrt{\ell}} - 1.5\frac{T}{\bar{t}^2}. \tag{12}$$

Upon writing $K_I = \sigma^\infty\sqrt{\pi a}$ and $T = -\sigma^\infty$, and letting σ_A attain the fracture strength σ_f, we have

$$\sigma_c = \sigma^\infty = \sigma_u\left[1 + \frac{4\sqrt{\pi}}{3}\bar{t}(a/\ell)^{1/2}\right]^{-1}, \tag{13}$$

where σ_u is given by Eq. (1). Consequently,

$$\bar{\sigma} = \frac{\sigma_c}{\sigma_u} = \left[1 + \frac{4\sqrt{\pi}}{3}\bar{t}(a/\ell)^{1/2}\right]^{-1}. \tag{14}$$

This prediction is included in Figure 5. It gives an excellent fit to the finite element predictions over the full range of $(\bar{t}^2 a/\ell)$ considered. This agreement is fortuitous at very small crack length. It is a consequence of the fact that the asymptote for the crack solution as $a \to 0$ happens to coincide with the unnotched strength. We argue that the domain of validity of the crack tip field is limited to $\bar{t}^2 a/\ell > 9/16\pi$, and to emphasise this, Eq. (14) is shown as a dotted line for $\bar{t}^2 a/\ell$ below this transition value.

In summary, an analytic model of the fracture toughness has been validated by FE simulations for the diamond-celled honeycomb. It is striking that the fracture toughness scales with $\bar{t}$ and not with $\bar{t}^2$: the honeycomb is remarkably tough. The FE simulations also reveal that the fracture criterion switches from K-control to strength-control with diminishing $\bar{t}^2 a/\ell$. The stress intensity factor is the appropriate failure parameter when a K-field exists on a larger scale than the cell size. But, when $\bar{t}^2 a/\ell$ is sufficiently small, no K-field exists due to the discreteness of the lattice. In fact, a negligible stress concentration is observed, and the unnotched strength σ_u is achieved.

The authors are grateful for the support provided by the EPSRC and by the European Community's Human Potential Programme HPRN-CT-2002-00198 (RTN-DEFINO).

[1] M.F. Ashby, Metall. Trans. 14A (1983) 1755.
[2] J.S. Huang, L.J. Gibson, Acta Metall. Mater. 39 (1991) 1617–1626.
[3] N.A. Fleck, X. Qiu., J. Mech. Phys. Solids, (2007) in press.
[4] L.J. Gibson, M.F. Ashby, Cellular Solids: Structure and Properties, 2nd ed., Pergamon Press, Oxford, 1999.
[5] N.A. Fleck, K.J. Kang, M.F. Ashby, Acta Metall. Mater. 42 (1994) 365–381.
[6] G.C. Sih, P.C. Paris, G.R. Irwin, Int. J. Fract. Mech. 1 (3) (1965).
[7] H. Tada, P.C. Paris, G.R. Irwin, The Stress Analysis of Cracks Handbook, Paris Productions, St. Louis, MO, 1985.
[8] S.G. Larsson, A.J. Carlsson, J. Mech. Phys. Solids 21 (1973) 263–277.